THE ASTROPHYSICAL JOURNAL, 280:580–591, 1984 May 15

THE KINEMATICS OF GIANT EXTRAGALACTIC H II REGIONS

EVAN D. SKILLMAN[1] AND BRUCE BALICK
Received 1983 July 25; accepted 1983 November 21

ABSTRACT

The kinematic structures of giant extragalactic H II regions in spiral galaxies, irregular galaxies, and "isolated extragalactic H II regions" are studied. Line profiles were found to be broad (FWHM > 30 km s^{-1}) throughout the core. Every region studied contains at least one "nucleus" with bright and, perhaps surprisingly, narrow emission lines. These data are discussed with regard to previous explanations for the large line widths observed in giant extragalactic H II regions.

Subject headings: galaxies: internal motions — nebulae: H II regions

I. INTRODUCTION

In 1970, Smith and Weedman first reported anomalously wide lines in giant extragalactic H II regions (hereafter GEHRs). When fitted to Gaussian profiles, their Hα line profiles showed full width at half-maximum (FWHM) as large as 60 km s^{-1}. Such velocities represent highly supersonic motions. Since then Melnick (1977) has discovered an empirical relationship between the line widths and linear diameters in giant extragalactic H II regions. In a more recent paper, Terlevich and Melnick (1981) show a tight relationship between Hα flux and line width. Nonetheless, the physical cause of these large line widths is still not clear.

Two different types of hypotheses have been proposed to explain the observations. Terlevich and Melnick believe that the line width is related to the total mass of the region through the virial theorem. In support of this, a graph is presented of corrected blue luminosity versus line width in which giant H II regions bridge the gap between globular clusters and the central bulges of spiral galaxies. A different explanation has been investigated by Dyson (1979). It is possible for the stellar winds of several young massive stars to form a shocked shell in the nearby ISM which can account for the broad line emission.

Observations using the Echelle spectrograph on the KPNO 4 meter telescope were conducted in order to distinguish between virial motions and winds from embedded stars. By observing at both high velocity resolution and high spatial resolution, it is possible to examine line profile shapes and how they change with radius in these H II regions. In the case of virialized motions, the high spatial resolution should allow the observations of individual clouds within the complex. The emission from each cloud should be narrow, and different clouds should be distributed throughout a range of velocities consistent with the large line widths of previous studies. For the stellar wind models, Dyson has calculated global line profiles for comparison to the circular aperture observations of Melnick. Those line profiles consist of two components: one broad line component of the shocked region; and a narrow line component of a surrounding region which has been ionized by UV photons escaping from the broad line region. In the Dyson model, the broad line emission should arise near the shell of a hot (10^6 K), highly ionized, wind-driven bubble. If the core consists of a single shell, and if that shell is resolved, then line splitting should be easy to detect. If the core is made up of several such shells, the line profile might be expected to exhibit small random variations across the face of the nebula.

In § II we present the echelle data. In § III we discuss our observations within the context of three different theoretical models: virialized motions, stellar winds, and the champagne flow model. The potential role of supernovae is also discussed. Section IV is a summary of our conclusions.

II. THE ECHELLE OBSERVATIONS

During the nights of 1980 March 28, 29, and 30 the echelle spectrograph on the Mayall 4 m telescope was used to observe giant H II regions in nearby spiral and irregular galaxies and "isolated extragalactic H II regions." The seeing varied between 2″ and 4″. The use of the long focus camera allowed a nominal spectral resolution of 2.55 Å mm^{-1}. The spatial resolution obtained was 11″ mm^{-1}. Baked IIIa-J photographic plates were used. An example of the data is shown in Figure 1; a 60 minute exposure of the giant H II region NGC 2363. Emission lines from [Ne III] λ3869 to Hα λ6563 are identified. (A detailed Hα exposure of NGC 2363 appears in Kennicutt, Balick, and Heckman 1980.) The slit was positioned E-W in order to cross the two brightest points in the nebula. Table 1 lists the relevent instrumental parameters.

The developed plates were digitized using the PDS microdensitometer at KPNO. A 10 × 10 μm aperture was used sampling at 10 μm increments. Selected emission lines

TABLE 1

INSTRUMENTAL PARAMETERS

Parameter	Value
Telescope	Mayall 4 m
Instrument	Echelle (red long focus camera)
Grating	31.6 l mm^{-1}
Cross disperser	100–1 first order
Slit width	100 μm
Dispersion at 5007 Å	2.56 Å mm^{-1}
Dispersion at 6563 Å	3.10 Å mm^{-1}
Spatial resolution	11.0 arcsec mm^{-1}
Instrumental profile	FWHM = 38 μm = 0.097 Å = 5.8 km s^{-1} at 5007 Å

[1] Visiting Astronomer, Kitt Peak National Observatory, which is operated by the Association of Universities for Research in Astronomy, Inc., under contract from the National Science Foundation.

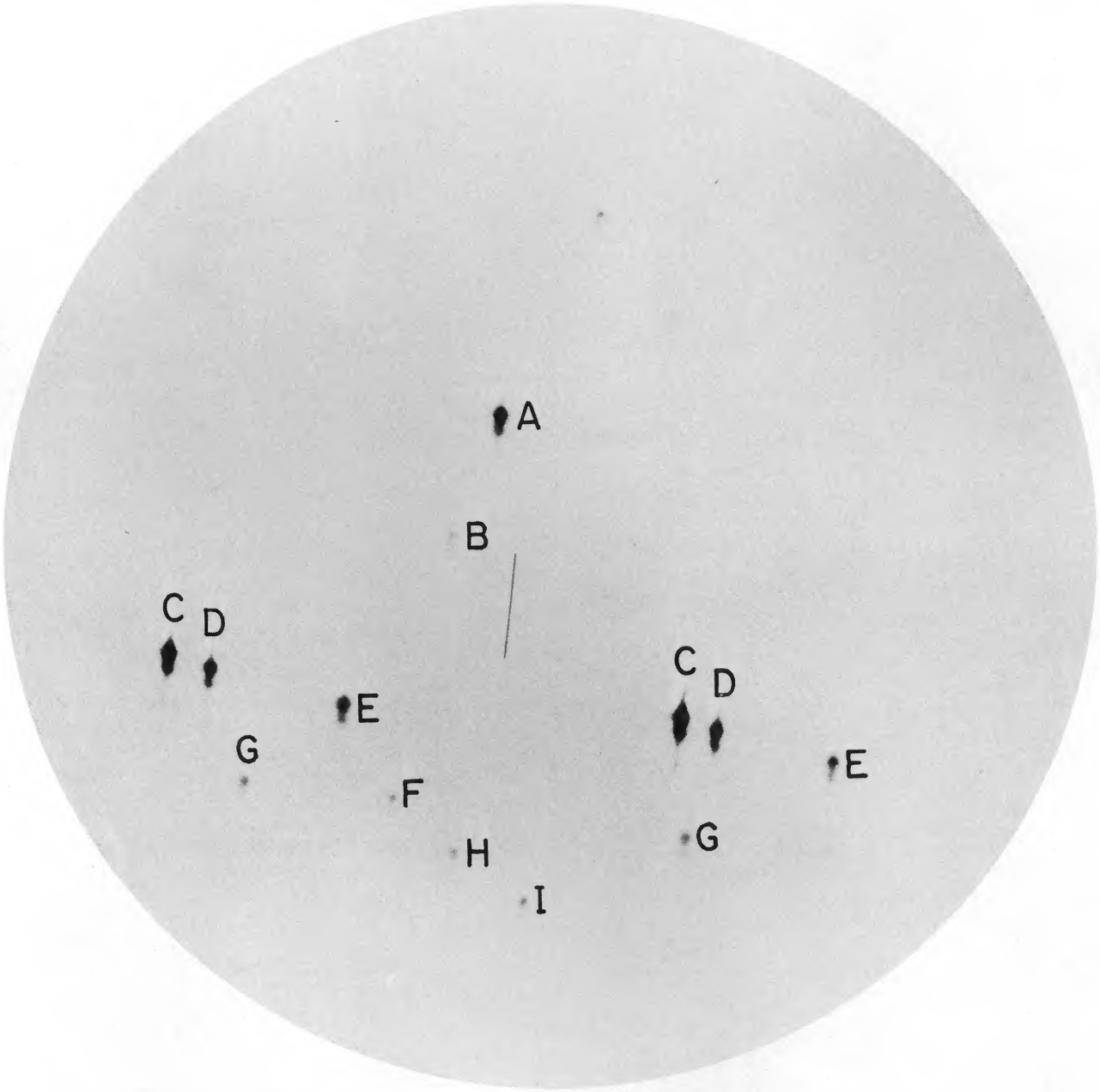

FIG. 1.—A 60 minute exposure of NGC 2363. The night sky line shows the length of the slit. The labels correspond to the following line identifications: A = Hα; B = He I λ5876; C = [O III] λ5007; D = [O III] λ4959; E = Hβ; F = [O III] λ4363; G = Hγ; H = Hδ; I = [Ne III] λ3869.

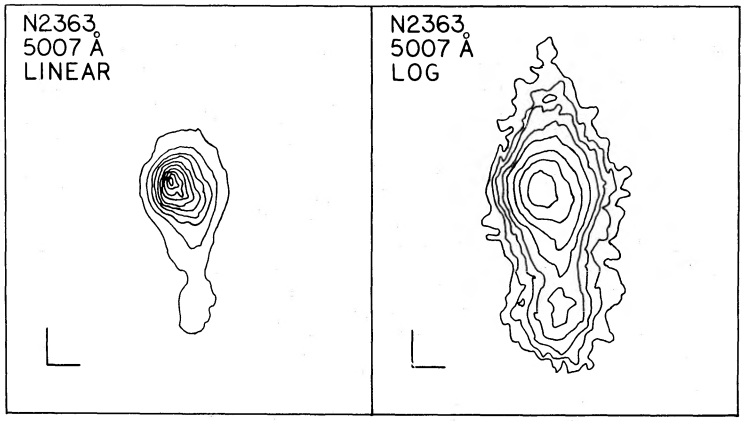

FIG. 2.—Logarithmic and linear contour plots of the 5007 Å line of NGC 2363. The reference bars measure 2″ along the slit (*vertical*) and 25 km s^{-1} across (*horizontal*).

were scanned along with the comparison "spot" plates. Densities were converted to intensities using the KPNO program on the IPPS. Figure 2 is a reproduction of the 5007 Å line of NGC 2363 (taken from a 5 minute exposure). The digitized data were block averaged over 4 pixels so that a single data point represents a 20×20 μm square of plate material. Using the UW microdensitometer, the dispersion and instrumental profile were determined from a He-Ar comparison source exposure. The 20 μm cell size represents a spatial element of 0.″22 and a velocity resolution of 3.1 km s^{-1} in the 5007 Å line.

Next, Gaussian profiles were fitted to the line shapes. In this procedure, adjacent rows were averaged so that a measurement of line width, center, amplitude, relative flux, and the rms of the fit were determined at every 0.″44. In the Gaussian fitting program, width, center, and amplitude were all treated as free parameters. In order to ensure the reliability of the derived parameters, single Gaussian fits were made of the 5007 Å and the 4959 Å lines of NGC 2363 from plates of 5, 30, and 60 minute exposure times. Gaussians fitted to these lines were found to be internally consistent except, of course, in cases where saturation affects the line peaks. As a second check, all of the rows of measureable flux were summed and fitted by a single Gaussian. This was done for a number of the H II regions observed and the widths determined in this manner showed good agreement with the line widths determined by Melnick (1977) using a Fabry-Perot. Exact agreement was not expected because of the considerable differences in geometry between the entrance apertures of the two instruments. Table 2 lists the objects observed.

a) NGC 2363

We will now present a detailed analysis of NGC 2363, the largest H II region in the Irr I galaxy NGC 2366. Figure 3 is a row by row graph of residuals of the single Gaussian fits to the 5007 Å line from the 5 minute exposure. From the systematic trends in the residuals it is clear that the line profiles are asymmetric in the region of highest flux. The fact that the asymmetry is strongest at the intensity maximum could simply be due to a decreasing signal-to-noise ratio in the regions of low intensity. However, analysis of the longer exposures shows that this asymmetry is actually limited to a small number of rows. These rows also distinguish themselves in plots of the log of the rms deviation of the fit versus the log of the flux. We conclude that the line

TABLE 2

JOURNAL OF OBSERVATIONS

Plate Number	Object Name	Exposure (minutes)	Position Angle (degrees)	Seeing (arcsec)
2880	N2363	30	E-W	4
2882	N2403 No. 1	40	E-W	3
2883	N4214 No. 1	60	E-W	3
2886	N5471	30	E-W	3
2888	II Zw 40	20	E-W	4
2889	N2363	60	E-W	4
2891	N3310 No. 1	23	E-W	3
2895	N4236 No. 1	90	+10	3
2896	N5461	40	+10	3
2897	N5455	56	+90	3
2898	N2363	5	E-W	2
2900	N2403 No. 3	60	+100	2
2901	N3239	70	+75	2
2905	N4861	5	+15	2
2906	N4861	30	+15	2
2908	II Zw 70	100	+95	2

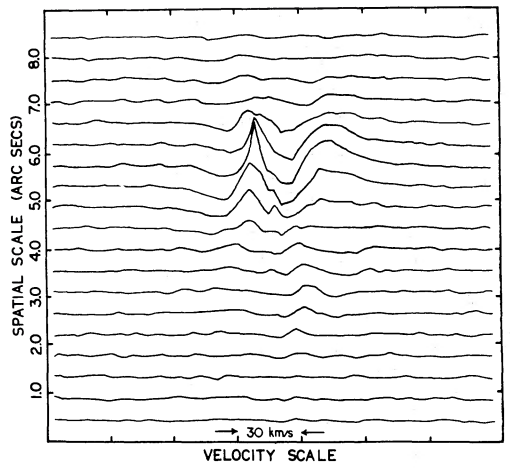

FIG. 3.—The residuals of single Gaussian fits to the 5007 Å line of NGC 2363. Each row represents 0.″44.

profiles are well represented by single Gaussians except for the region within 2″ of the intensity maximum. In these rows where the residuals warranted it, the line shape was fitted by two Gaussians. The results of the single and double Gaussian fits are shown in Figure 4 (*solid line* and *dashed line*, respectively). The profile widths reported here and throughout this paper are corrected for instrumental broadening, but not for thermal broadening. Although it is not clear that the source is uniquely described as two distinct Gaussian components, the asymmetric line profiles are fitted well in this manner, and the analysis was carried out under this assumption. As a reference, it is interesting to note that the spatial limit of our data is nearly identical to the core diameter of NGC 2363 of 11″ as measured by both Kennicutt (1979) and by Sandage and Tammann (1974); i.e., we are unable to detect line emission from the halo of the nebula.

The single Gaussian fits show that the [O III] emission is observed to be "broad" (FWHM > 30 km s^{-1}) throughout the core. The double Gaussians fitted to the asymmetric [O III] profiles in the bright center of the core of NGC 2363 yield a narrow line component and a broad line component separated by about 10 km s^{-1}. Within errors, the widths of both components show very little variation from row to row. The simplest interpretation is that of a narrow line component which has a larger systematic velocity of approximately 10 km s^{-1} relative to the broad line emission gas. Additionally, the narrow line emission gas is limited to a small spatial extent of about 3″, which suggests that this component may be unresolved. At a distance of 3.8 Mpc (Sandage and Tammann 1976), 1″ corresponds to 18 pc. As we proceed, we will refer to these regions of high flux and asymmetric profiles as nuclei. Note that this is a working definition and does not necessarily imply that the light recorded from the "nuclear" positions arises from a single phenomenon. In this spirit we construct a "nuclear profile" by summing over 2″ of slit centered on the region of asymmetric profiles. Figure 5 shows this profile along with single and double Gaussian fits and their respective residuals.

An identical analysis of the Hα emission line yields a somewhat surprising result. Figure 6 shows the results of row by row single Gaussian fits to the 60 minute Hα exposure, and Figure 7 is the nuclear profile constructed by summing over 2″ of slit in the region of the maximum intensity. The general trends in the flux, velocity, and width of the Hα line mimic those observed in the broad line component

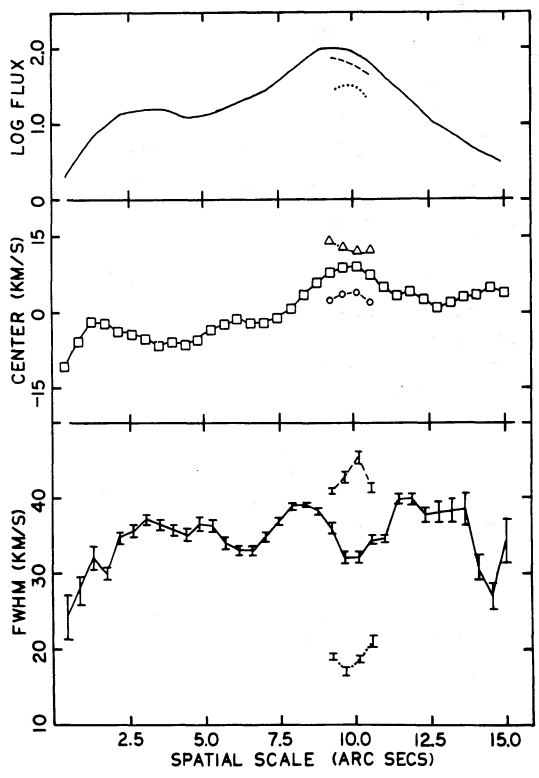

FIG. 4

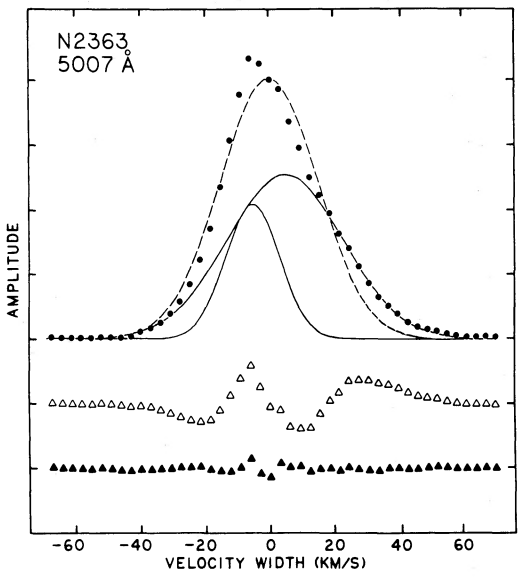

FIG. 5

FIG. 4.—The results of single and double Gaussian fits to the 5007 Å line of NGC 2363. The narrow component of the double Gaussian fits is represented by a dotted line and open triangles. The broad component is noted by a dashed line and open circles.

FIG. 5.—The nuclear profile for the 5007 Å line of NGC 2363 with the results of single and double Gaussian fits and their residuals. The broken line represents the single Gaussian fit to the data. The solid line shows the results of a double Gaussian fit. The open triangles show the residuals to the single Gaussian fit and the filled triangles show the residuals to the double Gaussian fit.

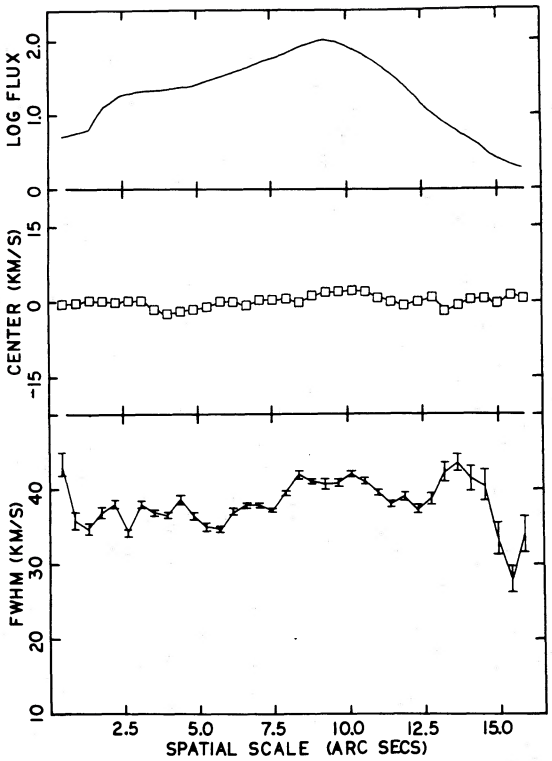

FIG. 6.—The results of single Gaussian fits to the Hα (6563 Å) line of NGC 2363.

of the 5007 Å line. However, there is no evidence of asymmetric profiles in either the row by row plots of the residuals or the nuclear profile. This can not be a signal-to-noise ratio effect, because the density of the Hα line in the 60 minute exposure is comparable to that of the 5007 Å line of the 5 minute exposure. The absence of an asymmetric profile in Hα cannot be explained by the larger thermal broadening of hydrogen relative to oxygen. We conclude that the relatively narrow nuclear [O III] emission may have no observable Hα counterpart.

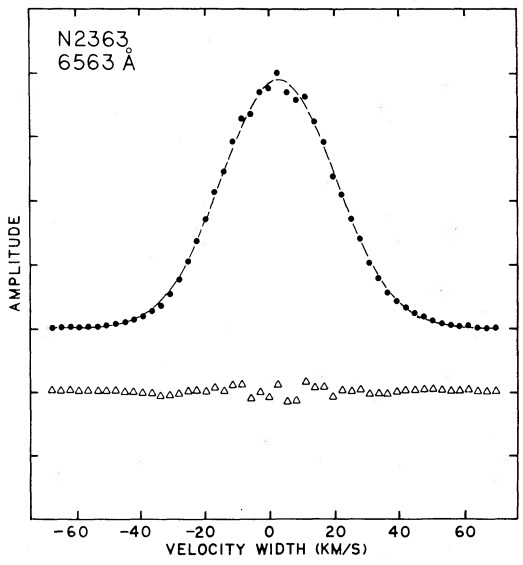

FIG. 7.—The nuclear profile for the Hα line of NGC 2363 showing the results of a fit to a single Gaussian.

More information can be obtained by directly comparing the [O III] and Hα emission lines. The ratio of the flux in the [O III] emission line to the flux in the Hα emission line was determined as a function of position. This was done by both comparing the results from the same exposure and comparing results from different exposures. Comparing data from the same exposure is most desirable because the results are free from variations in seeing and telescope positioning. However, comparing the [O III] data from the 5 minute exposure with the Hα data from the 60 minute exposure allows the best signal-to-noise ratio possible without the problem of saturation in the brightest regions. The results from both comparisons agreed at the qualitative level. Two characteristics were discovered. First, the [O III] line is strongest in the vicinity of the bright nucleus. Second, if the intensity of the narrow line component is subtracted from the [O III] profile, then the line ratio varies smoothly across the nucleus, and only slowly across the entire core.

The important point is that there exist differences in physical conditions between the nucleus and surrounding core. These differences are evidenced by both unique kinematic structure and significant variations in line strength ratios.

These observations of NGC 2363 suggest a simple model. The observed properties may arise from high temperature gas within the nucleus (at a velocity discrepant from the average velocity of the gas in the core), because the [O III] emission, but not the Hα, increases exponentially with temperature. (An increase in the gas temperature from 10,000 K to 20,000 K increases the $\lambda 5007/\lambda 6563$ emission ratio by a factor of 5.8.) Any explanation in which Hα is suppressed seems unlikely at temperatures less than 20,000 K. It is interesting to keep this model for NGC 2363 in mind while examining the data for the other regions.

b) NGC 5455

NGC 5455, a GEHR in M101, is an interesting case to compare and contrast with NGC 2363. Figure 8 shows contour plots of the 5007 Å line, and Figures 9 and 10 show the results of an analysis of NGC 5455 identical to that of NGC 2363.

The first notable difference between NGC 2363 and NGC 5455 is the appearance of symmetric profiles in the [O III] line at two different places along the slit. As in NGC 2363, the regions of asymmetric profiles distinguish themselves in plots of the log of the rms deviation of the fit versus the log of the flux. A second difference is that these asymmetric profiles are observed in both the 5007 Å line and the Hα line. The fact that these two nuclei are observed at two different intensities strengthens the belief that the spatial limitation of the asymmetric profiles is not an effect of the improved signal-to-noise ratio in the regions of highest intensity. Note also that the systematic velocity differences are opposite in sense when compared to NGC 2363: the narrow components of the double Gaussian fits lie at lower velocities than the wide component, although the velocity difference is small for the brighter nucleus. As in the case of NGC 2363, the relative strength of the [O III] emission increases in the nuclei.

At this point it would be most interesting to look at the ratio of the flux in the broad component to the flux in the narrow component for both the [O III] line and Hα. While

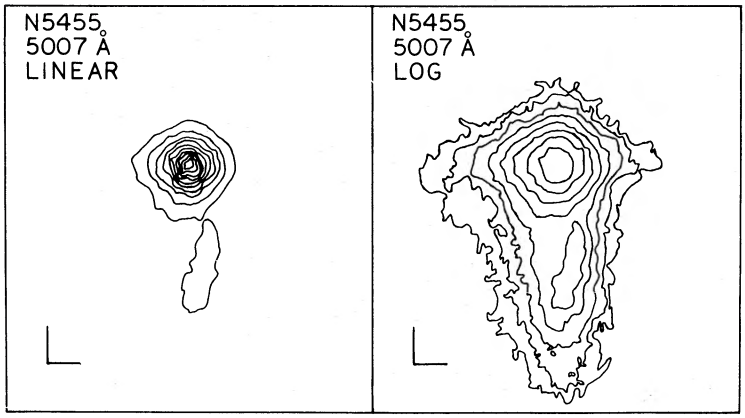

FIG. 8.—Logarithmic and linear contour plots of the 5007 Å line of NGC 5455

this is easily done, the results can be highly uncertain. Figures 11–14, the nuclear spectra for both nuclei in 5007 Å and 6563 Å, show why this is so. Qualitatively the [O III] lines are quite similar to the Hα lines. Attempts to compare the [O III]/Hα ratios in the nuclei are thwarted for two different reasons. In the fainter nucleus, the signal-to-noise ratio in the Hα line is insufficient to lend confidence to the relative line fluxes of the two components of the double Gaussian fit. In the brighter nucleus, the difference in center velocity between the broad and narrow components is small (less than the instrumental resolution). In this case, the line fluxes of the broad and narrow components cannot be clearly separated, i.e., the relative line fluxes of two fitted Gaussians can vary over an appreciable range with only a small effect on the rms deviation of the residuals.

c) Other Regions

Whereas many regions were well described by a single or double Gaussian fit, there were some regions showing more complex line profiles. NGC 5461 represents one such case in which the Hα nuclear profile revealed asymmetries quite unlike those in the [O III] nuclear profile. Obviously regions of this type cannot be interpreted in the same manner as the previous examples.

Every object studied in this survey showed evidence of one or more narrow line components in regions smaller than their broad line cores. All narrow line nuclei were of the order of a seeing disk in extent and spatially centered on flux maxima, although a few regions may have been confused by the juxtaposition of more than one nucleus.

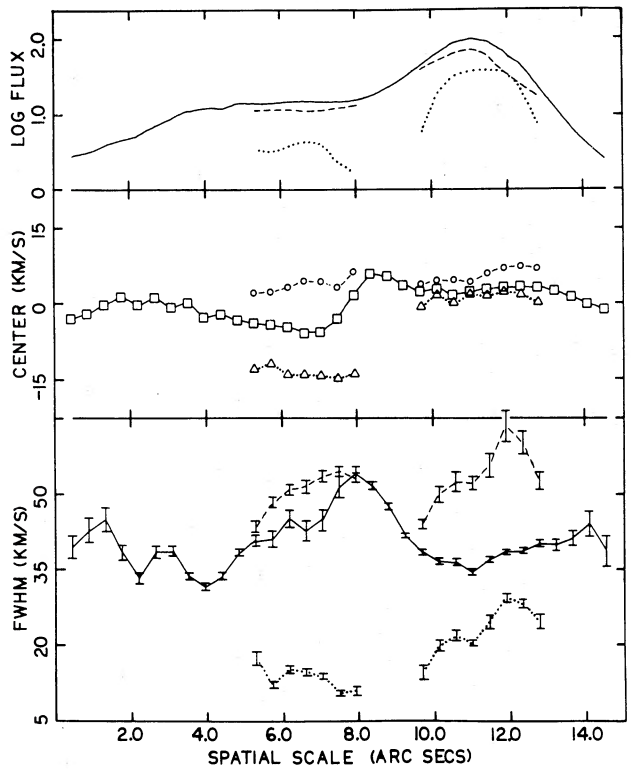

FIG. 9.—The results of the single and double Gaussian fits to the 5007 Å line of NGC 5455.

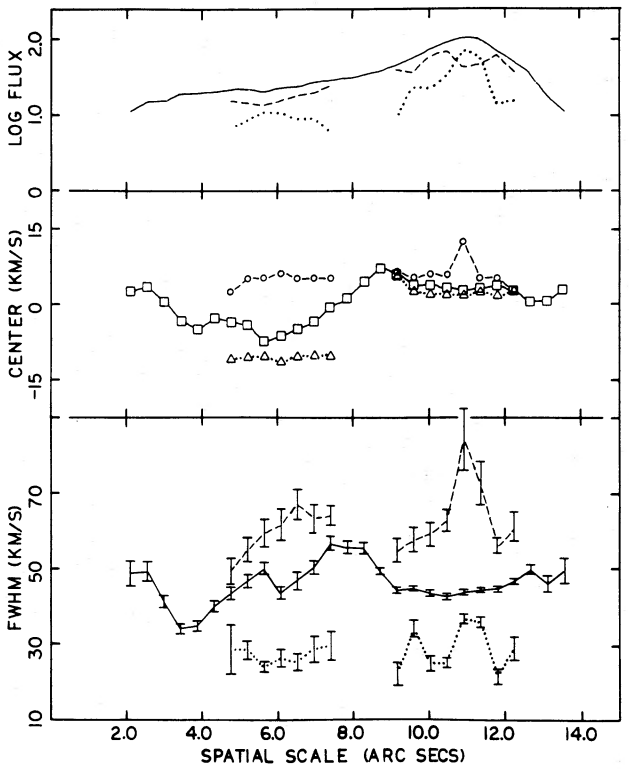

FIG. 10.—The results of the single and double Gaussian fits to the Hα (6563 Å) line of NGC 5455.

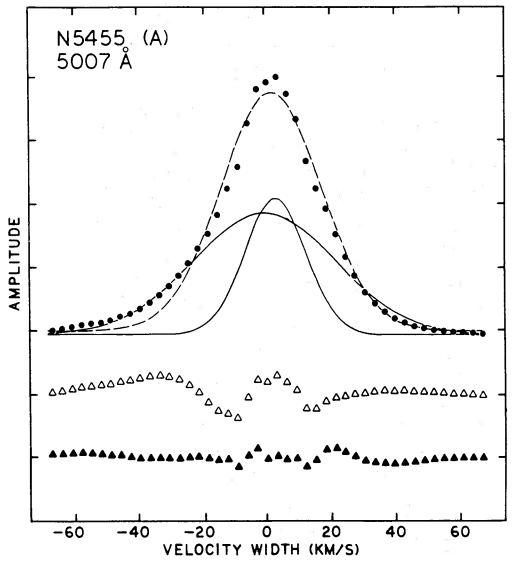

FIG. 11

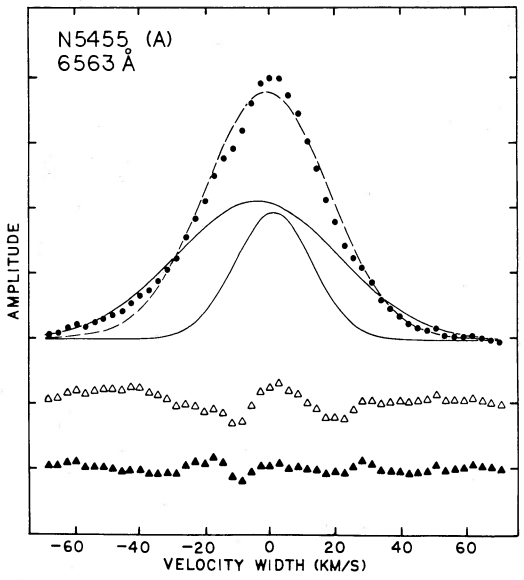

FIG. 12

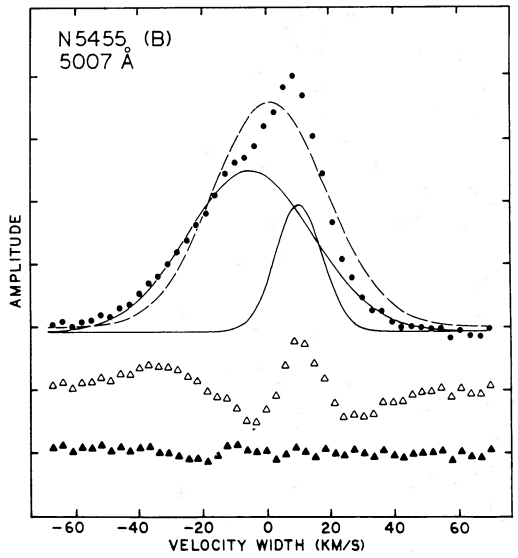

FIG. 13

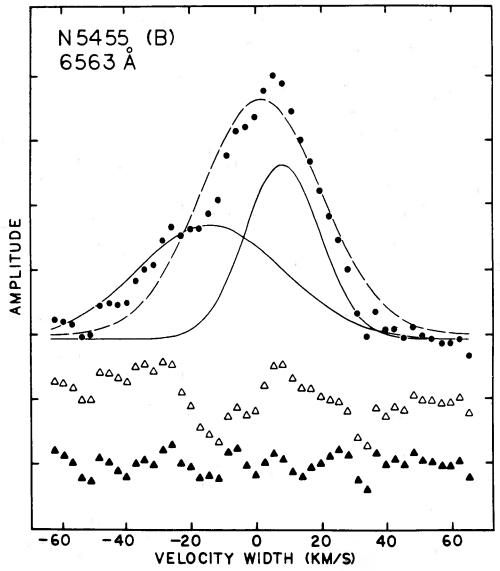

FIG. 14

FIGS. 11–14.—Nuclear profiles for the 5007 Å and 6563 Å lines of NGC 5455 for both nuclei.

The narrow line components could be found both redshifted and blueshifted relative to the broad line gas with typical systematic velocity differences ranging up to 15 km s^{-1}. For every GEHR studied, the single Gaussian fits were broad and showed little variation in centroid velocity out to the limit of our data. That limit always corresponded closely to the core diameter.

The above examples have shown that it is not adequate to use single Gaussian fits to determine the velocity dispersion of gas in a GEHR. This is demonstrated further by the 5007 Å line of NGC 4861 shown in Figure 15. Here it is obvious that a single Gaussian fit to the profile will be broadened by the displacement in velocity of separate components. The width of a Gaussian fit in this way will not be representative of the velocity dispersion of the gas. It may be that these separate components are physically unrelated. (At the distance of NGC 4861 [7.2 Mpc; Wakamatsu *et al.* 1979], the components have a projected separation of 100 pc.) Consequently any assumptions about the kinematic simplicity or asymmetry must be regarded skeptically.

In order to try to bring some coherence to a large and diverse data base, nuclear spectra were constructed for all of the objects observed. The results of Gaussian fits to these spectra have been compiled in Table 3. The spectra can be sorted into three different types: (1) those like NGC 2363 with strong asymmetries in [O III] but not in Hα; (2) those like NGC 5455 with similar asymmetries in both [O III] and Hα; and (3) those with complex asymmetries. As discussed earlier, for those objects with broad and narrow components

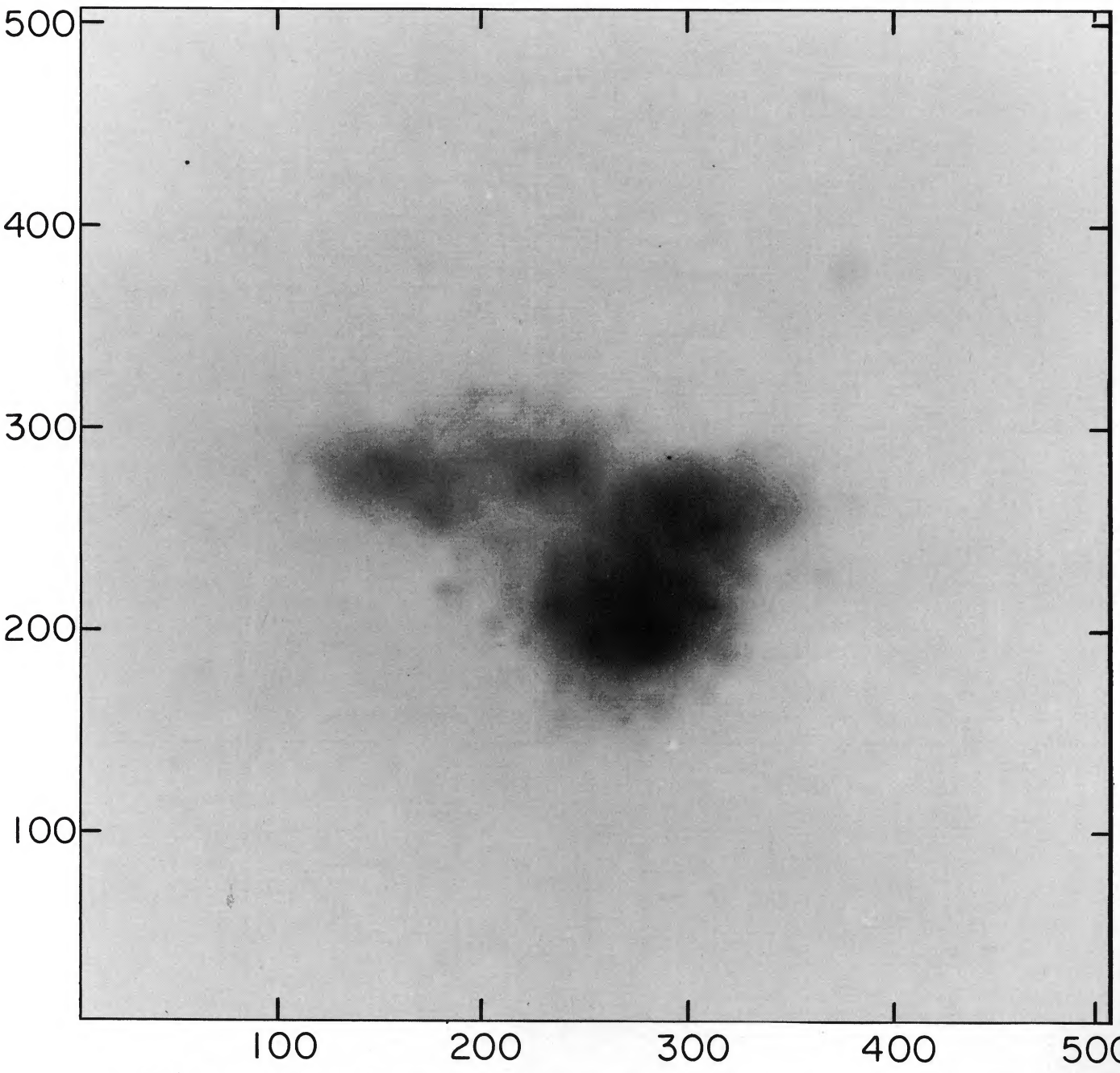

FIG. 15.—The 5007 Å line from NGC 4861. The original 64 × 64 pixel image has been enlarged 8 times to fill the 512 × 512 format of the Comtal video display.

TABLE 3

RESULTS OF FITS TO NUCLEAR SPECTRA

Region	FWHM Single (km s^{-1})	FWHM Narrow (km s^{-1})	FWHM Wide (km s^{-1})	FWHM Ratio (N/W)	Flux Ratio (N/W)	Δ Center (W-N) (km s^{-1})
N2363:						
λ6563	41.1(0.21)	...	...	...	...	...
λ5007	34.8(0.65)	18.3(0.41)	41.5(0.35)	0.45 ± 0.01	0.38 ± 0.02	10.2
N2403 No. 3:						
λ6563	36.2(0.38)	13.7(0.74)	37.9(0.25)	0.36 ± 0.02	0.09 ± 0.01	−8.6
λ5007	28.2(0.37)	12.6(0.32)	30.1(0.14)	0.42 ± 0.01	0.18 ± 0.01	−7.7
N3239 No. 1 (A):						
λ6563	44.7(0.45)	17.0(1.6)	48.7(0.66)	0.35 ± 0.03	0.08 ± 0.01	3.1
λ5007	35.6(0.36)	30.0(0.57)	61.2(3.0)	0.49 ± 0.03	1.8 ± 0.26	6.5
N3239 No. 1 (B):						
λ6563	47.5(0.29)	...	...	...	...	...
λ5007	44.4(0.36)	11.0(1.1)	46.6(0.36)	0.24 ± 0.02	0.04 ± 0.01	0.8
N3310 No. 1:						
λ6563	64.5(1.5)	50.4(2.6)	129.0(14.0)	0.39 ± 0.05	1.0 ± 0.22	16.2
λ5007	58.5(0.76)	49.8(1.1)	129.0(11.0)	0.39 ± 0.04	1.7 ± 0.29	0.1
N4214 No. 1 (B):						
λ6563	33.9(0.50)	17.8(3.1)	39.1(1.9)	0.45 ± 0.08	0.18 ± 0.07	0.1
λ5007	30.8(0.37)	22.9(0.51)	46.5(1.3)	0.49 ± 0.02	0.94 ± 0.09	−4.0
N4214 No. 1 (D):						
λ6563	28.8(0.33)	...	...	...	...	...
λ5007	22.3(0.23)	17.9(0.42)	31.9(0.98)	0.56 ± 0.02	1.4 ± 0.19	−5.3
N4236 No. 1:						
λ6563	55.2(1.1)	45.8(2.1)	110.0(14.0)	0.42 ± 0.06	1.4 ± 0.23	−15.5
λ5007	48.5(0.95)	26.0(1.3)	63.4(1.6)	0.41 ± 0.02	0.35 ± 0.03	−8.6
N5455 (A):						
λ6563	43.5(0.63)	27.1(1.4)	58.2(1.6)	0.46 ± 0.03	0.43 ± 0.05	−5.0
λ5007	36.2(0.58)	21.7(0.73)	51.9(1.2)	0.42 ± 0.02	0.48 ± 0.04	−3.4
N5455 (B):						
λ6563	43.0(1.3)	26.8(0.82)	52.7(3.4)	0.51 ± 0.04	0.79 ± 0.15	−19.5
λ5007	41.6(1.2)	16.5(0.67)	46.0(0.67)	0.36 ± 0.02	0.30 ± 0.02	−15.3
N5461:						
λ6563	44.8(0.74)	28.7(1.0)	70.4(2.6)	0.41 ± 0.02	0.58 ± 0.06	−1.0
λ5007	39.6(0.75)	28.7(1.2)	70.3(4.6)	0.41 ± 0.03	0.94 ± 0.15	5.2
N5471:						
λ6563	57.0(1.3)	36.7(11.0)	63.9(5.5)	0.57 ± 0.18	0.24 ± 0.20	7.4
λ5007	53.2(0.78)	23.0(1.1)	60.0(0.67)	0.38 ± 0.02	0.16 ± 0.01	9.3
II Zw 70:						
λ6563	44.4(0.66)	12.1(2.1)	47.2(0.82)	0.26 ± 0.04	0.04 ± 0.01	−3.1
λ5007	45.0(0.37)	34.9(2.3)	55.7(2.5)	0.63 ± 0.05	0.71 ± 0.22	−6.0

that are nearly coincident in velocity, the fits may be misleading. Thus, the relative ratios of [O III]/Hα emission for the double Gaussian fits are subject to systematic errors and may not always be significant.

The best cases in which to investigate the [O III]/Hα flux ratios are those for which both components of the double Gaussian fits for both lines show similar kinematics. For example, in NGC 2403 No. 3, the [O III] and Hα lines show comparable line widths for both components and similar velocity offsets of the component centers. The relative flux ratios indicate that the narrow component has an [O III]/Hα ratio of about twice that of the broad component. Overall, this trend applies to the other GEHRs in the same class.

III. DISCUSSION

a) *Virialized Motions*

Terlevich and Melnick (1981) have proposed that GEHRs are gravitationally bound systems and that the width of the nebular emission lines are a reflection of the depth of the gravitational potential. As evidence they show that the core radius (R_c) as measured by Sandage and Tammann varies approximately as the second power of the emission line width. This is similar to relationships derived for globular clusters, elliptical galaxies, and the bulges of spiral galaxies. Similarly, that the Hβ flux was shown to be proportional to the fourth power of the line width is taken as evidence that the same physical processes dominate the kinematics of these objects.

In the Terlevich and Melnick model of a GEHR, "the observed emission line profile widths represent the velocity dispersion of ionized gas clouds moving in the overall gravitational potential of gas and stars." In order to explain our observations of narrow line nuclei within the context of the Melnick and Terlevich model would require a certain fraction of the exciting stars in the center of the core to be constrained to a small range of velocities while the rest of the exciting stars showed a much larger velocity dispersion. The only satisfactory explanation requires that the narrow line emission arises in a single cloud.

The observations of broad emission line profiles throughout the core requires that a number of clouds must be observed along each line of sight. It is then interesting to investigate lifetimes of such clouds. A calculation has been made in the

Appendix that demonstrates that the clouds can survive without collisions for lifetimes comparable to the lifetimes of the exciting stars.

To further compare the spatial variation of line width of the broad line gas with the theoretical model requires caution. The variation of velocity dispersion with radius for relaxed, gravitationally bound, systems has been calculated by King (1966), and a comparison of the present Echelle data with this model might provide a consistency check. However, the definition of core radius for relaxed systems corresponds approximately to the half-power width of the luminosity distribution, and the core radius for GEHRs as measured by Sandage and Tammann corresponds to a steep decrease in surface brightness that can represent a radius many times larger than the half-power width of the luminosity distribution. If the two definitions are assumed to be equivalent for the sake of comparison, then the fact that the line width of the broad line gas is approximately constant to the extent of our measurements may be consistent with a King model. This is because the velocity dispersion does not decrease significantly within one core radius in the King models. Since the limit of the present data roughly corresponds to the core radius, the lack of variation of line width with radius will not provide a discriminating test. It would be most interesting to observe the variation of line width with radius beyond the core and into the halo.

b) *Stellar Winds*

Dyson (1979) has proposed that the broad nebular lines may be the result of the motions of shells of shocked gas driven by the stellar winds of the young massive stars in the centers of GEHRs. In his models, the stellar winds of many stars coelesce to form giant "bubbles." The velocity of the thin shell of shocked gas resulting from the interaction of the stellar wind with the surrounding gas can exceed the local sound speed. Dyson has shown that this scheme is energetically feasible.

Observational support already exists for this theory. Conti and Massey (1981) and D'Odorico and Rosa (1981) have discovered evidence for large numbers of W-R stars in the GEHR of M33. Rosa and D'Odorico (1982) point to the existence of ring structures which they claim are most likely not formed by supernovae. Since 30 Doradus has also been shown to have numerous W-R stars and ring-type structures, Rosa and D'Odorico suggest that all giant H II regions may have a common basis. Using assumptions for W-R stellar mass loss and lifetimes, they show that a reasonable number (50) of W-R stars can account for the total mechanical energy content of a GEHR.

Our data raise some difficulties for the stellar wind interpretation. The narrow line component cannot be easily explained in the model of a wind-blown bubble. The temperature inside the bubble is too hot for O^{++} to exist, and thus the narrow line emission would have to originate outside of the bubble. If a bubble were resolved, one would expect line splitting originating from the front and rear of the shell along the line of sight. Only in one or two cases do we find a profile that could be easily interpreted as line splitting. Note that Rosa and D'Odorico find an average shell radius of 25 pc which would be unresolved or close to the resolution limit for many of our observations.

The present data might be accomodated within the W-R bubble model if a few narrow line filaments surround the bubble's exterior. The narrow line component of the nucleus is then a region where the slit of the echelle happens to cross a particularly bright filament. The velocity disparities among nuclei are comparable to those observed in the well-studied galactic W-R bubble nebulae (Schneps *et al.* 1981; Chu 1982; Treffers and Chu 1982). Deep photographs of the GEHRs are needed in order to establish whether such bright filaments are common. In the cases of NGC 2363 and the GEHRs of M101 such a model seems very unlikely based on available Hα photographs (Hodge and Kennicutt 1983).

c) *Champagne Flows*

There is one model that can account for both a narrow line nuclear component and broad lines. The numerical calculations of Tenorio-Tagle (1979) (and other papers in the series) have shown that flows with velocities in excess of 30 km s^{-1} can be created when an H II region is formed near the edge of a giant molecular cloud. In this model, pressure differences between the high density region of star formation and the surrounding low density medium can give rise to a temporary supersonic expansion of the H II region. Unlike the stellar wind case, the temperature of the gas immediately surrounding the exciting stars is compatible with the presence of O^{++}. The nucleus corresponds to a high density zone immediately adjacent to the exciting star, and the broad line core consists of gas flowing from the nucleus. The magnitudes of the line widths and nucleus-core systemic velocity differences as well as their respective spatial extents are adequately explained by the model.

Melnick (1980) states that the velocity dispersion must increase with distance from the core in order for the champagne model to be valid. Because he measures the velocity dispersion in the halo of NGC 604 to be significantly less than in the core, he rules out the champagne model as a reasonable explanation for the large line width of the core. This condition would require that the flow persists out into the halo of the region. If, instead, one assumes that the flow reaches a terminal velocity within the core, then the conflict with his observations is resolved. The only other published data on the kinematics of the halo of a GEHR comes from a Fabry-Perot study of the Hα emission line of 30 Doradus (Smith and Weedman 1972). Even relatively small aperture observations (~4 pc) of the halo gas produce broad profiles (FWHM > 40 km s^{-1}). Again, we emphasize that there is a need for kinematic studies of the halo gas of GEHRs in the present sample.

There are two alternative ways of viewing the echelle data within the context of a champagne flow model. If the double Gaussian profiles are to be interpreted as two distinct components, then the narrow component would be associated with the high density and relatively quiescent gas surrounding the exciting stars, and the broad component would be a result of the turbulent supersonic flow into the lower pressure ISM. The fact that the narrow line component is sometimes found redshifted relative to the broad line component presents a problem, as it is difficult to see how the flow could be directed away from the observer and yet the region of the exciting stars still remain visible. On the other hand, the profiles may not be true Gaussians, but just asymmetric. Champagne flows should produce asymmetric profiles.

The champagne flow model requires that star formation in

GEHR occurs at the edges of dense molecular clouds. Thus, observations of CO in GEHRs are important to this discussion. Elmegreen, Elmegreen, and Morris (1980) observed the NGC 2363 region in a survey of irregular galaxies and obtained a null result. On the other hand, Blitz *et al.* (1981) discovered the largest CO cloud known to date coincident with the GEHR NGC 5461 in M101. The limitations of resolving power and sensitivity of current CO observations may leave this an unanswered question for quite some time.

d) The Potential Role of Supernovae

The large velocity widths associated with GEHR imply a total energy content of the gas of 10^{51}–10^{52} ergs. The previous sections have discussed the possibility of gravitational potential energy, stellar winds, or gas flows as a source of this energy. It is also possible that one or more supernovae may impart a significant fraction of this energy to the gas. Benvenuti, D'Odorico, and Dumontel (1979) discuss the results of a steady state calculation for NGC 604 that, generalized, indicates that more supernovae should be present in GEHR than are currently detected. They suggest that their calculation may be at fault due to the presence of a single extremely luminous ($M \sim -9$) star. This would affect their estimate of the number of high mass stars implied by the total ionizing flux. D'Odorico and Rosa (1981) suggest that the NGC 604 region may be so young that the most massive stars have not yet had time to evolve to the supernova stage. In this case a steady state calculation would be inappropriate.

We would like to note here one other possibility; that supernovae may be hidden within GEHR. There are three standard tests for finding extragalactic SNR. The first is the strength of the [S II] lines relative to Hα. The second is the indication of high gas temperature (>20,000 K) from the temperature-sensitive [O III] $\lambda 4363/(\lambda 5007 + \lambda 4959)$ ratio. The third is the presence of a nonthermal, unresolved radio continuum source. It is possible to imagine a supernova within a GEHR which is not detectable in any of these ways using standard observational techniques.

e) A Comparison with 30 Doradus

The 30 Doradus region in the Large Magellanic Cloud is the best studied of all GEHRs and may help us to better interpret the present observations. A difficulty lies in adjusting to the factor of 60 (minimum) improvement in resolution. The low resolution Balmer-line photometry of Strauss, Braz, and Ducati (1979) leads us to the conclusion that, viewed at the distance of the rest of our sample, 30 Doradus would be judged to have only one nucleus. From Smith and Weedman (1972) we find that a 2′ aperture centered on this nuclear region (their position 336) produced an [O III] profile with two components offset by about 20 km s^{-1}. This aperture covered several bright filaments, which, observed with a smaller aperture, show a range in velocities of 68 km s^{-1}. If 30 Doradus is a typical GEHR, this would imply that our nuclear profiles may represent the integration of light from several independent structures.

IV. CONCLUSIONS

We have studied the kinematics of a number of GEHR and find the following:

1. The line profiles are not well represented by single Gaussians. A narrow component or asymmetry exists in every region studied.
2. These narrow components can be displaced in velocity in either a positive or negative manner. Because of this a single Gaussian fit to the profile may not be a good representation of the inherent velocity dispersion of the gas.
3. The region of asymmetric profiles appears to be spatially limited to a size much smaller than the core of the region. For this reason, we have chosen to call them nuclei. In many cases our data are consistent with an unresolved nucleus corresponding to a size of less than 50 pc.
4. The asymmetries are always more pronounced in the [O III] emission line profiles than the Hα emission-line profiles.
5. When fit by single Gaussians, the emission lines are broad throughout the core of the region.
6. All of the explanations for the large line widths of GEHR suffer some deficiencies in explaining our data (some more than others) unless ad hoc assumptions are invoked.

In light of the importance of GEHR to extragalactic research, we point to the need for a better understanding of the physical nature of these objects.

We gratefully acknowledge assistance from Rob Kennicutt, Caty Pilachowski, and Paul Hodge during the preparation stages of this project. Doug Tody and Ken Mighell made valuable contributions to the data reduction process.

APPENDIX

In the model proposed by Terlevich and Melnick, a GEHR should consist of a gravitationally bound assemblage of ionized gas clouds. The broad emission lines are therefore due to the line-of-sight contributions of many gas clouds at different velocities. Since the emission is well represented by a single broad Gaussian throughout most of the core of the GEHR, many individual gas clouds (~10) must contribute along each line of sight. If these clouds interact with one another or with some sort of intercloud medium, then viscosity will lead to a general collapse of the system. Thus the question becomes one of the mean time between cloud-cloud collisions in the absence of an intercloud medium.

We can investigate the consequences of our observations on this model by considering the GEHR NGC 2363 in some detail. We will model the core of NGC 2363 as a spherical volume with a diameter of 10″. With a seeing disk of 2″ there would be 25 resolution elements across the face of the nebula. In order for the emission-line profile to be well fitted by a single Gaussian would require each resolution element to include the contribution of 10 ionized clouds. This sets a lower limit of about 200 for the number of clouds in the region. From the observations of Kennicutt, Balick, and Heckman (1980), we take as a filling factor for the ionized gas 3×10^{-3}. If we assume spherical ionized clouds of a uniform size, we can then calculate a cloud radius of 2.5 pc. From $n_e = 500$ cm^{-3} (Kennicutt *et al.*) we can calculate that each cloud must receive the ionizing flux of the equivalent of three O5 stars. Thus the total ionizing flux

of the model is within a factor of 2 of that observed, which, considering the simplicity of the model, is quite satisfactory.

Accepting 10 km s^{-1} as an rms velocity along the line of sight, and therefore 17 km s^{-1} as an rms space velocity (u) for the ionized clouds, then the collision frequency per cloud (z) can be estimated from

$$z = \sqrt{2}N\pi D^2 u ,$$

where N is the number density of ionized clouds and D is the cloud diameter. For this model $N = 2.5 \times 10^{-5}$ cm^{-3} and $z = 10^{-8}$ yr^{-1}.

This picture is viable in terms of both the estimated sizes of the ionized gas clouds and the small collision frequency necessary to allow the numerous clouds to exist at discrepant velocities. However, we have assumed that the gas cloud is totally ionized. The filling factor that we have used is for the ionized gas. This requires a very low density of neutral gas between the ionized gas clouds to prevent high Mach number turbulence from dissipating the mechanical energy. Since the core of the GEHR represents the deepest point in the gravitational potential proposed in the Terlevich and Melnick model, it is difficult to justify such a small filling factor for the sum of the neutral and ionized gas in the central region.

REFERENCES

Benvenuti, P., D'Odorico, S., and Dumontel, M. 1979, *Ap. Space Sci.*, **66**, 39.
Blitz, L., Israel, F. P., Neugebauer, G., Gatley, I., Lee, T. J., and Beattie, D. H. 1981, *Ap. J.*, **249**, 76.
Chu, Y.-H. 1982, *Ap. J.*, **254**, 578.
Conti, P. S., and Massey, P. 1981, *Ap. J.*, **249**, 471.
D'Odorico, S., and Rosa, M. 1981, *Ap. J.*, **248**, 1015.
Dyson, J. E. 1979, *Astr. Ap.*, **73**, 132.
Elmegreen, B. G., Elmegreen, D. M., and Morris, M. 1980, *Ap. J.*, **240**, 455.
Hodge, P. W., and Kennicutt, R. C. 1983, *A.J.*, **88**, 296.
Kennicutt, R. C. 1979, *Ap. J.*, **228**, 394.
Kennicutt, R., Balick, B., and Heckman, T. 1980, *Pub. A.S.P.*, **92**, 134.
King, I. R. 1966, *A.J.*, **71**, 64.
Melnick, J. 1977, *Ap. J.*, **213**, 15.
———. 1980, *Astr. Ap.*, **86**, 304.
Rosa, M., and D'Odorico, S. 1982, *Astr. Ap.*, **108**, 339.
Sandage, A., and Tammann, G. A. 1974, *Ap. J.*, **190**, 525.
———. 1976, *Ap. J.*, **210**, 7.
Schneps, M. H., Haschick, A. D., Wright, E. L., and Barrett, A. H. 1981, *Ap. J.*, **243**, 184.
Smith. M. G., and Weedman, D. W. 1970, *Ap. J.*, **161**, 33.
———. 1972, *Ap. J.*, **172**, 307.
Strauss, F. M., Braz, M. A., and Ducati, J. R. 1979, *Astr. Ap.*, **74**, 280.
Tenorio-Tagle, G. 1979, *Astr. Ap.*, **71**, 59.
Terlevich, R., and Melnick, J. 1981, *M.N.R.A.S.*, **195**, 839.
Treffers, R., and Chu, Y.-H. 1982, *Ap. J.*, **254**, 569.
Wakamatsu, K., Sakka, K., Nishida, M., and Jugaku, J. 1979, *Pub. Astr. Soc. Japan*, **31**, 635.

BRUCE BALICK and EVAN D. SKILLMAN: Astronomy Department, FM-20, University of Washington, Seattle, WA 98195